

## Design of Compact and Wideband Suppression Low Pass Elliptic Filter by n-Segment Step Impedance Transmission Line

M. Hayati<sup>1</sup>, M. Amiri<sup>1</sup>, and S. H. Sedighy<sup>2</sup>

<sup>1</sup> Department of Electrical Engineering  
Razi University, Kermanshah, Iran  
hayati@razi.ac.ir, mozhgan.amiri@gmail.com

<sup>2</sup> School of New Technologies  
Iran University of Science and Technology, Tehran, Iran  
sedighy@iust.ac.ir

**Abstract**— In this paper, the invasive weed optimization technique for compacting a microstrip elliptic low pass filter is proposed and validated. At the first step, the invasive weed optimization (IWO) technique is used to replace the shunt resonators transmission lines of the conventional filter with arbitrary n-segments Step Impedance Transmission Lines (SITLs) for compacting it. To validate the proposed method, the shunt resonator transmission lines of a seventh-order elliptic lowpass filter are replaced with proper SITLs which cause more than 30% compactness in this step. Then the IWO technique is applied on the general filter configuration to design a wideband harmonic suppression and compact elliptic low pass filter. This method extends the stop band bandwidth more than 8.5  $f_0$  and also increases the compactness to 47%. The measurement results of the final optimized fabricated filter are in good agreement with the simulation ones.

**Index Terms** — Elliptic low pass filter, harmonic suppression, Invasive Weed Optimization (IWO), microstrip, miniaturization, wideband.

### I. INTRODUCTION

A microstrip lowpass filter with small size, sharp transition band and wide stopband is frequently used in the modern microwave and millimeter wave communication system to suppress harmonics and unwanted signals. There are several techniques for designing low pass filters such as Butterworth, Chebyshev, elliptic function, all pass, and Gaussian response. In the elliptic filters, the response has equal-ripple in both the pass band and stopband, which means that the elliptic function design is superior to both the Butterworth and Chebyshev designs. Moreover, these filters have sharp cutoff skirts and low in-band insertion loss [1-5].

The elliptic function low pass filters show the advantages of high performance, low cost, capability of implementation with microstrip technology and easy fabrication [1,2]. Also elliptic filters achieve the smallest filter order for the same specifications and the narrowest transition width for the same filter order compared to other filter design techniques. The microstrip realization of elliptic filter can be implemented with several configurations of microstrip transmission lines such as shunt stubs and stepped impedances [1,2]. Due to the rapid development of wireless communication technology, miniaturization receives a high demand in the designing of microwave devices, especially filters [6]. The conventional microstrip low pass filters techniques such as shunt stubs or high–low impedance transmission lines have been widely used in microwave systems for their remarkable characteristics [3]. However, it is hard to achieve compact size and high performance simultaneously with these implementation methods [3]. Also, the conventional low pass filters (LPFs) can only provide a gradual transition and a narrow stopband [1]. Moreover, raising the filter's order can improve its performance which enlarges the overall filter size and increases the insertion loss.

To reduce the physical size of microstrip filters, many approaches have been investigated and commonly used in the circuit designs such as stepped-impedance resonator (SIR) [7], defected ground structure (DGS) [8], photonic band gap structure (PBG) [9,10], metamaterial [11], quasi-lumped element [12], and dual-mode/half-mode resonator [6]. Photonic bandgap and defected ground structures can provide sharp and extended stopband in the LPF [13-15]. However, these techniques cause many disadvantages such as complex configuration and fabrication difficulties [13]. The LPFs using defected ground structures have been proposed in [16] and [17]. In [16], a quarter-circle defected ground

structure shape was introduced, despite its wide stopband with very good insertion and return losses, it suffers the large size and gradual transition band. A quasi-elliptic LPF using three DGS units and a compensated microstrip line has been designed and implemented in [17], which has high insertion loss and narrow stopband. A lowpass filter using stepped impedance compact microstrip resonator cell (SICMRC) has been proposed in [18]. The SICMRC has been embedded in the structure of double arrow shaped microstrip cell (DASMC) to obtain a sharp response. Although it is compact LPF with wide stopband, it isn't sharp adequately. A compact elliptic-function low-pass filter by etching stepped impedance resonators (SIR) in the back substrate side has been presented in [19], which it suffers the narrow stop bandwidth. A microstrip lowpass filter with a novel patch resonator consisting of a semi-circle and semi-ellipse loaded by delta stub and rhomboid structures has been studied in [20], which has the gradual transition band with large size. In [21], a compact microstrip stepped impedance lowpass filter using back-to-back C-shaped and triple C-shaped thin slots has been presented which has wide stopband, but its frequency response is not sharp sufficiently in the transition band and does not have good passband performance due to its significant insertion loss. A LPF using circular hairpin resonator has been designed in [22] which has a compact size, but it doesn't have good insertion loss, sharp roll off and wide stop band.

In [23], the uniform transmission line segments of a low pass filter have been replaced by step impedance transmission lines optimized by invasive weed optimization (IWO) technique. In this paper, the IWO algorithm is used to compact the conventional elliptic low pass filter and increase the harmonic suppression bandwidth. For this purpose, the shunt resonators which have  $m$ -segments transmission lines are replaced with proper compact arbitrary  $n$ -segments step impedance transmission lines in a seventh-order lowpass elliptic filter configuration. The simulation results show more than 30% compactness compared with the conventional one. Then, the IWO technique is applied on the general filter structure to design a compact wideband harmonic suppression elliptic low pass filter. The designed filter has 3 dB cut off frequency at 3.2 GHz. Moreover, the optimized filter has area reduction about 47% and the harmonic suppression about  $8.5f_0$ . Finally, the optimized filter is fabricated. The measurement results are in good agreement with the simulation ones.

## II. COMPACT SITL ELLIPTIC LPF

In this section, replacing method of  $m$ -segments step impedance transmission lines with  $n$ -segments SITLs by using the IWO technique is discussed. Then, this technique is applied in a seventh-order lowpass elliptic filter to miniaturize the overall filter size. This section is

organized as follows. At first, the formulation of an arbitrary  $n$ -segment SITLs is presented and equaled with  $m$ -segments SITLs to extract the problem equations. Then, the IWO is used to find the best responses which satisfy the equations with the most compact size. Finally, the proposed optimized SITLs method is used to compact a conventional seventh order elliptic LPF.

### A. Formulation of an arbitrary SITL

Step impedance transmission line (SITL) is a non-uniform transmission line which can be used in the microstrip circuits to reduce its overall size, shift the spurious pass band to the higher frequency, and even to suppress the multiple spurious pass bands [23,24]. Figure 1 illustrates the non-uniform  $m$ -segments transmission lines with the electrical length and characteristic impedance of the  $\theta_i$  and  $Z_i$  for the  $i$ -th segment which should be equal to non-uniform transmission lines with arbitrary  $n$ -segments at the design frequency,  $f_0$ . As depicted in Fig. 1, the compact SITL configuration is constructed from the  $n$  transmission line segment with the electrical length and characteristic impedance of the  $\theta'_i$  and  $Z'_i$  for the  $i$ -th segment.

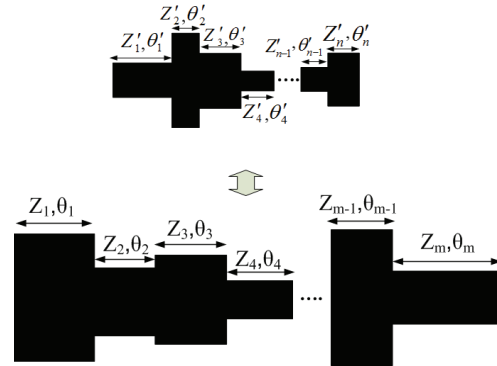


Fig. 1. Equivalent of  $m$ -segments step impedance transmission lines with arbitrary  $n$ -segments SITLs.

The ABCD matrix of the SITLs is obtained by multiplying the ABCD matrixes of all  $m$  or  $n$ -segments. Therefore, to equate these two mentioned structures, the ABCD matrixes of them should be equal with each other at the design frequency,  $f_0$ , as follows:

$$\begin{aligned}
 [ABCD]^{mSITL} &= \\
 &\begin{bmatrix} \cos \theta_1 & jZ_1 \sin \theta_1 \\ j \sin \theta_1 / Z_1 & \cos \theta_1 \end{bmatrix} \times \begin{bmatrix} \cos \theta_2 & jZ_2 \sin \theta_2 \\ j \sin \theta_2 / Z_2 & \cos \theta_2 \end{bmatrix} \times \\
 &\dots \times \begin{bmatrix} \cos \theta_m & jZ_m \sin \theta_m \\ j \sin \theta_m / Z_m & \cos \theta_m \end{bmatrix} = \begin{bmatrix} \cos \theta'_1 & jZ'_1 \sin \theta'_1 \\ j \sin \theta'_1 / Z'_1 & \cos \theta'_1 \end{bmatrix}, \quad (1) \\
 &\times \begin{bmatrix} \cos \theta'_2 & jZ'_2 \sin \theta'_2 \\ j \sin \theta'_2 / Z'_2 & \cos \theta'_2 \end{bmatrix} \times \dots \times \begin{bmatrix} \cos \theta'_n & jZ'_n \sin \theta'_n \\ j \sin \theta'_n / Z'_n & \cos \theta'_n \end{bmatrix} \\
 &= [ABCD]^{nSITL}
 \end{aligned}$$

where “ $m$ SITL” and “ $n$ SITL” stand for  $m$ -step and  $n$ -step impedance transmission lines, respectively. As it can be seen, there are 3 equations with  $2n$ -unknown variables in (1) which are  $Z'_1 \sim Z'_n$  and  $\theta'_1 \sim \theta'_n$ . Therefore, there are a lot of response groups which can satisfy the equations. Notice that since the structure is reciprocal, there are only three independent equations [1]. To achieve the most compact equivalent SITLs, the invasive weed optimization can be used which is described in the next section.

### B. Invasive weed optimization

IWO is a simple numerical stochastic search algorithm that mimics the natural behavior of weed colonizing in the opportunity spaces for optimizing the function. However, it has been shown to be effective in converging to an optimal solution by employing basic properties such as seeding, growth, and competition in a weed colony. Some basic properties of the process are as follows [24]:

- 1) *Initialization*: A population of initial seeds ( $N_0$ ) is randomly being dispread over the search area.
- 2) *Reproduction*: The individuals, after growing, are allowed to reproduce new seeds linearly based on their fitness, the lowest and the highest fitness of the colony (all of plants). Note that maximum ( $S_{max}$ ) and minimum ( $S_{min}$ ) number of seeds are predefined parameters of the algorithm and fitted according to structure of problem. The procedure is demonstrated in Fig. 2 [25].
- 3) *Spatial Dispersal*: The generated seeds are being randomly spread with a normal distribution over the search area.
- 4) *Competitive Exclusion*: When the maximum number of plants in a colony is obtained ( $P_{max}$ ), each weed is allowed to produce seeds and scatter them according to its fitness. Then, new seeds with their parents are categorized together with respect to their fitness. Next, weeds with lower fitness are eliminated to reach the maximum determined population size in a colony.
- 5) *Termination Condition*: The whole process continues until the maximum number of iterations has been obtained, the plant with the best fitness is the closest one to the optimal solution [26].

In this section, the optimization goal is the equalization of the non-uniform  $m$ -segments transmission lines with a  $n$ -segment step transmission lines. For this purpose, the ABCD matrixes of  $m$ -segments transmission lines are compared with  $n$ -segment step transmission lines as described in Sec. II.A and construct the error function as:

$$error = \sqrt{e_A^2 + e_B^2 + e_C^2}, \quad (2)$$

where

$$e_A = A^{mSITL} - A^{nSITL}, \quad (3)$$

$$e_B = B^{mSITL} - B^{nSITL}, \quad (4)$$

$$e_C = C^{mSITL} - C^{nSITL}. \quad (5)$$

The goal of the design is to minimize the error in (2) with the smallest electrical length. The fitness function of this objective can be expressed as:

$$f = w_1 e - w_2 \theta_T, \quad (6)$$

where  $\theta_T$  is the total electrical length of the  $m$ -segments SITL and  $w_1$  and  $w_2$  are the weighting coefficients. By choosing the weighting coefficients, one can decide the importance of the  $m$ -segments SITL and  $n$ -segments SITL equalization against the compactness. In other words, choosing the  $w_1/w_2 > 1$  puts the goal of optimization on the compacting of the transmission line rather than the equalization of  $m$ -segments SITL with  $n$ -segments SITL. Notice that the equalization importance of  $m$ -segments SITL and  $n$ -segments SITL is related to the structure that the transmission line wants to be employed on it.

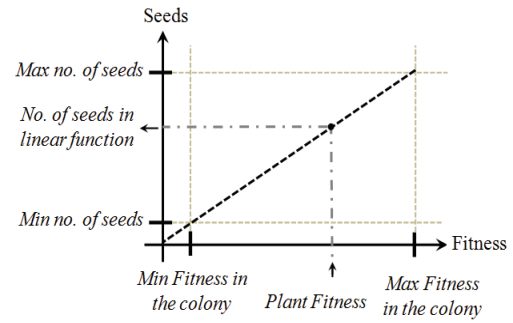


Fig. 2. Seed production procedure in a colony of weeds versus the fitness.

### C. Simulation and results

In this section, a compact seventh-order lowpass elliptic filter is designed and simulated by using the  $n$ -SITLs. For this purpose, a conventional elliptic low pass filter is designed firstly. Then, the three 2-segments resonators of the conventional elliptic filter are replaced with the SITLs to validate the proposed technique in a practical miniaturization. An elliptic lowpass prototype filter with pass band ripple  $L_{Ar}=0.1$  dB and a minimum stop band attenuation  $L_{As}=86.9778$  dB at  $\Omega_s=1.8182$  for the  $\Omega_e=1.8182$  is chosen, where element values are  $g_0=g_s=1$ ,  $g_1=1.141$ ,  $g_2=1.369$ ,  $g_2'=0.0479$ ,  $g_3=1.9472$ ,  $g_4=1.4033$ ,  $g_4'=0.1408$ ,  $g_5=1.8107$ ,  $g_6=1.1316$ ,  $g_6'=0.1408$ ,  $g_7=0.9616$  [1]. The microstrip LPF is designed to have a 3 dB cut off frequency at 3.2 GHz and source/load impedance  $Z_0=50 \Omega$ . The microstrip realization is performed by using RT/Duroid 5880 substrate with the dielectric constant of 2.2 and a thickness of 20 mil. Also, all of the inductors are realized by using high-impedance lines with characteristic

impedance of  $Z_{OL}=164 \Omega$ , whereas the all capacitors are realized by using low-impedance lines with characteristic impedance  $Z_{OC}=19 \Omega$ . Figure 3 (a) shows the layout of the designed LPF, which all the electrical lengths are denoted in Table 1. Notice that the superscript ‘‘P’’ stands for the ‘‘prototype’’ in the indexes. Also, the overall prototype LPF size is  $25.2 \text{ mm} \times 10.3 \text{ mm}$ . Moreover, as demonstrated in Fig. 3 (a), two shunt resonant branches are realized with two high and low impedance microstrip lines segments in the both sides of the filter structure.

Figure 3 (b) illustrates the elliptic LPF which its shunt resonators with two SITLs segments are replaced with 3 or 4 segments SITLs. Notice that here the superscript ‘‘O’’ is stand for the ‘‘optimized’’ in the indexes. The optimized values of the SITLs are computed by the IWO method based on the formula presented in Sec. II.B. Moreover, the IWO algorithm parameters are shown in Table 2. As exhibited in the Table 3,  $13 \Omega$  and  $164 \Omega$  are chosen as the lower and higher limitation of the impedances research area. Also, the 1 and 90 degrees are selected as the interval of the electrical length variables. This interval guarantees the global optimum finding of the problem. Since the run time of the algorithm is very low, the number of initial population and maximum number of plant population are selected as high as 80 to achieve more accuracy in the method. Moreover, by choosing  $\sigma_{final}=0.01$ , the error level can be decreased and more precise results may be achieved. The equivalents SITLs for each shunt resonant branch are obtained based on the resonance frequency of it. The resonance frequencies of the three shunt resonators of the designed prototype filter are  $f_{r1}=12.49 \text{ GHz}$ ,  $f_{r2}=7.19 \text{ GHz}$  and  $f_{r3}=8.02 \text{ GHz}$ . The final values of the optimized electrical lengths and characteristic impedances of the transmission lines at the design frequency,  $f_0$ , are specified in Table 3.

Figure 4 shows the comparison between full wave simulation of the prototype and optimized LPF done by commercial microwave circuit simulator Agilent Advance Design System (ADS). As it can be seen, there is a good agreement between the prototype and compact design filters. The physical size of the optimized LPF is  $22 \times 8.1 \text{ mm}^2$ . It implies that the IWO technique decreases the circuit size of the filter about 30%. Although this size reduction is good, it is possible to achieve more compactness. We discussed about it in the next section.

Table 1: Values of prototype LPF electrical lengths

Parameter	$\theta_1^p$	$\theta_2^p$	$\theta_3^p$	$\theta_4^p$	$\theta_5^p$
Value (rad)	0.355	0.113	1.105	0.632	0.095
Parameter	$\theta_6^p$	$\theta_7^p$	$\theta_8^p$	$\theta_9^p$	$\theta_{10}^p$
Value (rad)	1.325	0.589	0.215	0.565	0.303

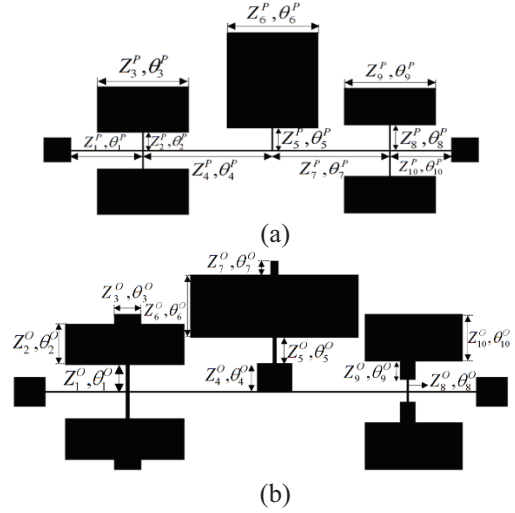


Fig. 3. (a) Prototype elliptic LPF, and (b) elliptic LPF with SITL.

Table 2: IWO parameters

Symbols	Quantity	Value
$N$	Number of initial population	80
$iter_{max}$	Maximum number of iterations	72
$D$	Problem dimension	6, 8
$P_{max}$	Maximum number of plant population	80
$S_{max}$	Maximum number of seeds	10
$S_{min}$	Minimum number of seeds	2
$n$	Nonlinear modulation index	3
$\sigma_{initial}$	Initial value of standard deviation	1
$\sigma_{final}$	Final value of standard deviation	0.01
$Z_i$	Impedance of the lines	$19 < Z_i < 164$
$\theta_i$	Electrical length of the lines	$0.5 < \theta_i < 190$

Table 3: Values of the proposed compact SITL LPF

Parameter	$Z_1^o$	$Z_2^o$	$Z_3^o$	$Z_4^o$	$Z_5^o$
Value ( $\Omega$ )	130.989	17.003	55.5374	46.6154	125.957
Parameter	$Z_6^o$	$Z_7^o$	$Z_8^o$	$Z_9^o$	$Z_{10}^o$
Value ( $\Omega$ )	13.0077	133.241	163.929	13.0665	56.104
Parameter	$\theta_1^o$	$\theta_2^o$	$\theta_3^o$	$\theta_4^o$	$\theta_5^o$
Value (rad)	0.1751	0.845	0.0821	0.1634	0.0411
Parameter	$\theta_6^o$	$\theta_7^o$	$\theta_8^o$	$\theta_9^o$	$\theta_{10}^o$
Value (rad)	0.6982	0.0707	0.2358	0.344	0.0642

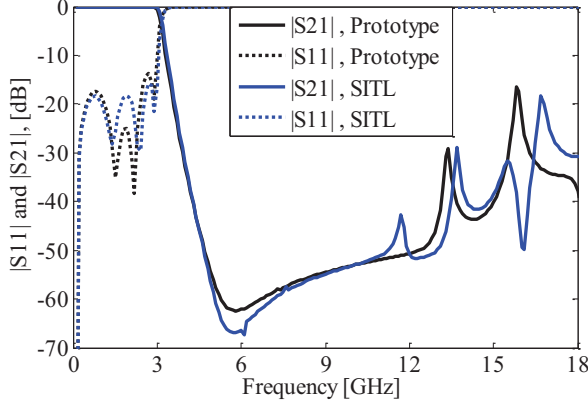


Fig. 4. Full wave simulation results of the prototype LPF and SITL LPF.

### III. OPTIMIZATION OF WIDEBAND HARMONIC SUPPRESSION ELLIPTIC LOW PASS FILTER

In this section, we aim to achieve much more compactness and wideband harmonic suppression in the elliptic low pass filter by using IWO technique. For this purpose, first the ABCD matrix of the general compact filter shown in Fig. 3 (b) is extracted. Then the scattering parameters of it are calculated by using the ABCD matrix technique.

#### A. Formulation of the ABCD matrix of the general filter structure

From the ABCD matrix point of view, the filter layout in Fig. 3 (b) is composed of 4 cascaded high impedance transmission lines with 3 shunt impedance between them which its circuit is shown in Fig. 5. In more details, the resonant branches can be considered as shunt impedance which is located between two transmission line segments. To find these shunt impedances, the end open transmission line segment of them can be considered as the load of the previous line as depicted in Fig. 5. As an example, this calculation is done for the first shunt resonator of the filter. The impedance of an open end step can be calculated by:

$$Z_{in1}^{SH1} = \frac{Z_3^F}{j \tan \theta_3^F}, \quad (7)$$

where  $Z_3^F$  and  $\theta_3^F$  are the characteristic impedance and the electrical length of the open end transmission line, respectively. Also the whole impedance of the each open end step transmission line with previous segment can be calculated by:

$$Z_{in2}^{SH2} = Z_2^F \frac{Z_{in1}^{SH1} + jZ_2^F \tan \theta_2^F}{Z_2^F + jZ_{in1}^{SH1} \tan \theta_2^F}, \quad (8)$$

where  $Z_2^F$  and  $\theta_2^F$  are the characteristic impedance and the electrical length of the second segment, respectively.

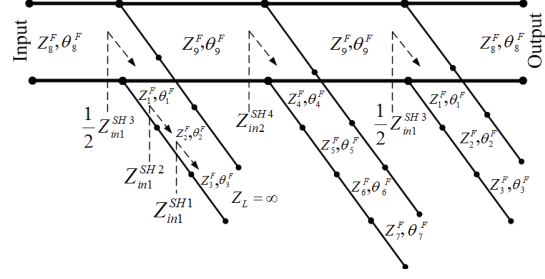


Fig. 5. Finding the input impedance of the shunt SITL resonators.

Similarly, the other transmission line steps can be considered as the load impedance for previous one. Therefore, the impedance of the 3 sequential steps can be calculated as follows:

$$Z_{in3}^{SH3} = Z_3^F \frac{Z_{in2}^{SH2} + jZ_3^F \tan \theta_3^F}{Z_3^F + jZ_{in2}^{SH2} \tan \theta_3^F}, \quad (9)$$

where  $Z_3^F$  and  $\theta_3^F$  are the characteristic impedance and the electrical length of the third transmission line. Notice that, the first and the last shunt resonators are placed on the both sides of the filter layout and therefore we consider them divided by two in the circuit and formulation. This process is iterated to achieve all the input impedance of the shunt SITL resonators. Then each of these resonator branches is considered between the cascaded transmissions lines with the ABCD matrix as follows [1]:

$$\begin{bmatrix} A & B \\ C & D \end{bmatrix} = \begin{bmatrix} 1 & 0 \\ 1/Z_{ini}^{SH} & 1 \end{bmatrix}. \quad (10)$$

Notice that, to decrease the number of the variables, the filter configuration is considered as a symmetrical structure. Therefore, we have two different shunt resonators, the first one with 3 segments (6 variables) and the middle one with the 4 segments (8 variables), and two different horizontal line (4 variables). Now, the ABCD matrix of the general structure can be obtained by multiplying the ABCD matrix of all cascaded parts which are computed as:

$$\begin{aligned} ABCD^{LPF} &= \begin{bmatrix} \cos \theta_8^F & jZ_8^F \sin \theta_8^F \\ j \sin \theta_8^F / Z_8^F & \cos \theta_8^F \end{bmatrix} \times \begin{bmatrix} 1 & 0 \\ 2/Z_{in1}^{SH3} & 1 \end{bmatrix} \times \\ &\times \begin{bmatrix} \cos \theta_9^F & jZ_9^F \sin \theta_9^F \\ j \sin \theta_9^F / Z_9^F & \cos \theta_9^F \end{bmatrix} \times \begin{bmatrix} 1 & 0 \\ 1/Z_{in2}^{SH4} & 1 \end{bmatrix} \times \\ &\times \begin{bmatrix} \cos \theta_9^F & jZ_9^F \sin \theta_9^F \\ j \sin \theta_9^F / Z_9^F & \cos \theta_9^F \end{bmatrix} \times \begin{bmatrix} 1 & 0 \\ 2/Z_{in1}^{SH3} & 1 \end{bmatrix} \times \\ &\times \begin{bmatrix} \cos \theta_8^F & jZ_8^F \sin \theta_8^F \\ j \sin \theta_8^F / Z_8^F & \cos \theta_8^F \end{bmatrix} \end{aligned}, \quad (11)$$

where  $Z_8^F, Z_9^F$  and  $\theta_8^F, \theta_9^F$  are the characteristic impedances and the electrical lengths of the 4 cascaded high impedance transmission lines and  $Z_{in1}^{SH3}, Z_{in2}^{SH4}$  are the input impedance of the series-resonant branches. According to (12) and (13), the S-Parameters of the filter are given in the terms of SITLs electrical lengths and characteristic impedances as follows [1]:

$$S_{21} = \frac{2}{A + B/Z_0 + CZ_0 + D}, \quad (12)$$

$$S_{11} = \frac{A + B/Z_0 - CZ_0 - D}{A + B/Z_0 + CZ_0 + D}. \quad (13)$$

Since the electrical length of a transmission line changes versus frequency linearly, the electrical length  $\theta_i$  in a different frequency ( $f_i$ ), can be calculated as:

$$\theta_i = \theta_0 \frac{f_i}{f_{3dB}}, \quad (14)$$

where  $\theta_0$  is the electrical length in the 3 dB cut off frequency ( $f_{3dB}$ ). This relation can be used to achieve the ABCD matrix of the filter versus frequencies.

## B. IWO description

The IWO algorithm has been explained in the previous section. Here we want to use the IWO to achieve a compact and high order suppression filter presented in Sec. III.A. For this purpose, the scattering matrix of the general proposed filter structure introduced in the previous section should compare with the desired low pass filter response. The desired lowpass filter response shown in Fig. 6 with blue color. As it can be seen, the desired response has very high order suppression. The IWO tries to adapt the response of the general filter structure with the desired one. In other words, the IWO should minimize the error function of this adaption which can be expressed as:

$$error = \sqrt{\left(|S_{11}^{design}| - |S_{11}^{desired}|\right)^2 + \left(|S_{12}^{design}| - |S_{12}^{desired}|\right)^2}, \quad (15)$$

where the  $|S_{11}|$  and  $|S_{12}|$  are the vector of the sampled data. Notice that the -20 dB in  $f < f_{3dB}$  and -15 dB in  $f > f_{3dB}$  in Fig. 6 are chosen as thresholds for  $|S_{11}|$  and  $|S_{12}|$ , respectively. In other words,  $|S_{11}|$  and  $|S_{12}|$  below these values in the corresponding regions don't make any change in the error value. The IWO parameters are tabulated in Table 4.

The final results of the optimized electrical lengths and characteristic impedances for the compact and wideband suppression SITL LPF are tabulated in Table 5. The full wave simulation results of the final optimized SITL LPF are demonstrated in the Fig. 6 with black color. As it can be seen, the simulation results of the optimized SITL LPF has good compatibility with the desired response in the pass band and stop band areas.

Table 4: IWO parameters

Symbols	Quantity	Value
$N$	Number of initial population	80
$iter_{max}$	Maximum number of iterations	72
$D$	Problem dimension	18
$P_{max}$	Maximum number of plant population	80
$S_{max}$	Maximum number of seeds	10
$S_{min}$	Minimum number of seeds	2
$n$	Nonlinear modulation index	3
$\sigma_{initial}$	Initial value of standard deviation	1
$\sigma_{final}$	Final value of standard deviation	0.01
$Z_i$	Impedance of the lines, Ohm	$19 < Z_i < 164$
$\theta_i$	Electrical length of the lines, degree	$0.5 < \theta_i < 90$

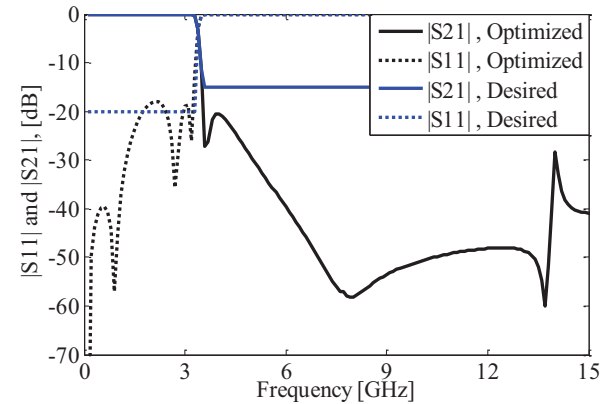


Fig. 6. The desired response for elliptic low pass filter and full wave simulation result of the optimized SITL LPF.

Table 5: Values of wideband SITL LPF

Parameter	$Z_1^F$	$Z_2^F$	$Z_3^F$	$Z_4^F$	$Z_5^F$
Value ( $\Omega$ )	164.004	62.1178	19.6982	164.004	58.9093
Parameter	$Z_6^F$	$Z_7^F$	$Z_8^F$	$Z_9^F$	-
Value ( $\Omega$ )	27.0067	58.9093	164.004	164.004	-
Parameter	$\theta_1^F$	$\theta_2^F$	$\theta_3^F$	$\theta_4^F$	$\theta_5^F$
Value (rad)	0.026	0.01819	0.25759	0.59803	0.33738
Parameter	$\theta_6^F$	$\theta_7^F$	$\theta_8^F$	$\theta_9^F$	-
Value (rad)	0.11323	0.09118	0.25135	0.31202	-

### C. Fabrication and measurement

Figure 7 illustrates the fabricated compact and wideband suppression elliptic optimized LPF. As it can be seen, the meandering techniques have been applied to the middle high-impedance section of the proposed LPF to reduce the overall circuit size. The optimized SITL LPF is fabricated on RT/Duroid 5880 substrate with the relative dielectric constant of 2.2, thickness of 20 mil and loss tangent of 0.0009. The measurements were performed by the HP 8757A network analyzer. The EM simulation and measured S-Parameters of the proposed LPF are shown in Fig. 8 (a), which indicates a good agreement between them. The final physical size of the designed LPF is 13.3 mm × 10.3 mm, which is 47% less than the prototype LPF. The maximum insertion loss is only 0.1dB in the passband and the rejection band extends from 3.34 GHz to 27 GHz with the attenuation level better than 15 dB, whereas the prototype LPF rejection band is only 12.8 GHz. In other words, the proposed filter has about 23.66 GHz reject bandwidth compared with the traditional LPF which has 12 GHz reject bandwidth. The transition band of the proposed LPF is only 0.16 GHz from 3.2 GHz to 3.36 GHz with corresponding attenuation levels of -3 dB and -20 dB, respectively while the prototype LPF transition band is 0.47 GHz. In other words, the optimized filter has a sharp roll off response. Also, the insertion loss is less than 0.1 dB from DC to 3.14 GHz (98.12% of the passband region). The group delay of the designed LPF in the pass band region is shown in Fig. 8 (b). It can be seen that the maximum variation is less than 0.85 ns which is negligible.

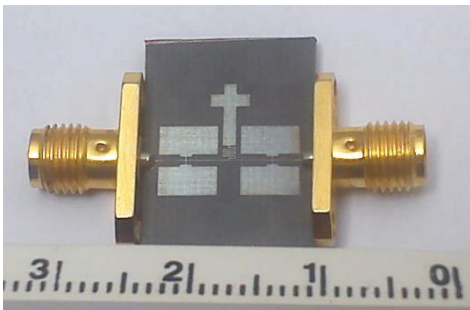


Fig. 7. Fabricated wide band suppression elliptic LPF.

The performance of the proposed LPF is compared with some other published works in Table 6, where  $f_c$  is 3 dB cut off frequency and  $\zeta$  is the roll-off rate that is used to evaluate the sharpness of transition band, which is defined as [27]:

$$\zeta = \frac{\alpha_{\max} - \alpha_{\min}}{f_s - f_c}, \quad (16)$$

where  $\alpha_{\max}$  is the -20 dB attenuation point,  $\alpha_{\min}$  is the -3 dB attenuation point,  $f_s$  is the -20 dB stopband frequency

and  $f_c$  is the -3 dB cutoff frequency. The relative stopband bandwidth (RSB) is calculated by [28]:

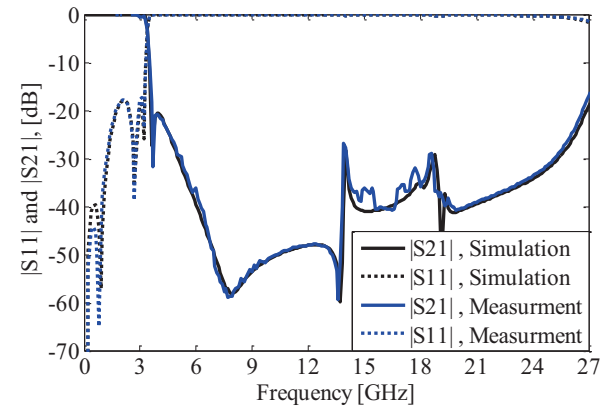
$$RSB = \frac{\text{stopband}(-20\text{dB})}{\text{stopband center frequency}}. \quad (17)$$

The suppression factor (SF) is dependent upon the stopband suppression. A higher suppression degree in the stopband leads to a greater SF. For example, if the stopband bandwidth is calculated under -40 dB limitation, then the SF is considered as 4. Also, the normalized circuit size (NCS) is formulated as [27]:

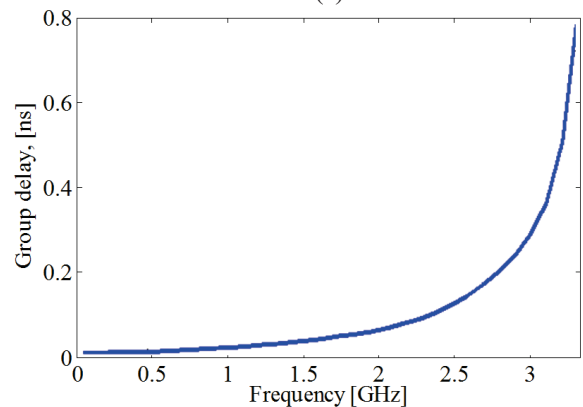
$$NCS = \frac{\text{physical size (length} \times \text{width)}}{\lambda_g^2}. \quad (18)$$

This is used to obtain the degree of miniaturization of a filter, where  $\lambda_g$  is the guided wavelength at -3 dB cutoff frequency. The architecture factor (AF) can be identified as the circuit complexity factor, which is signed as 1 when the design is 2D and as 2 when the design is 3D. Eventually, the figure-of-merit (FOM) of a filter is defined as [28]:

$$FOM = \frac{\xi \times RSB \times SF}{NCS \times AF}. \quad (19)$$



(a)



(b)

Fig. 8. (a) EM simulation and measurement results of the fabricated filter, and (b) the group delay of the fabricated filter.

Table 6: Performance comparison of the proposed LPF with other published works

Ref.	$f_c$ (GHz)	$\zeta$	RSB	NCS	FOM
[16]	2.95	12.1	1.28	0.093	500
[17]	1.87	130	1.16	0.0827	3775
[18]	5.8	23	1.45	0.07	1100
[19]	1	130	0.98	0.0042	6010
[20]	3.12	35.7	1.351	0.0508	1900
[21]	2	28.3	1.3	0.0128	5754
[22]	2.5	27.4	0.6	0.0148	2518
This Work	3.2	106	1.54	0.0295	12500

According to Table 6, the proposed lowpass filter has good compactness and excellent RSB as well as higher roll-off rate and FOM among the published works.

#### IV. CONCLUSION

The invasive weed optimization was applied on the non-uniform  $m$ -segments transmission line to compact it, by replacing with  $n$ -segments step impedance transmission lines. Then the proposed method was implied on transmission lines of a seventh-order lowpass elliptic filter to reduce the circuit size. The results showed about 30% compactness. In the next step, the IWO technique was used to design a wideband harmonic suppression elliptic low pass filter based on the extracted layout in the previous section. The proposed filter was simulated, fabricated and measured. The measurement results were in good agreement with the simulation results and showed the stop band bandwidth more than  $8.5 f_0$  and about 47% compactness. Also, this technique can be use in the design of other microwave devices.

#### REFERENCES

- [1] J. S. Hong and M. J. Lancaster, *Microstrip Filters for RF/Microwave Applications*, Wiley, New York, 2001.
- [2] G. D. Vendelin, A. M. Pavio, and U. L. Rohde, *Microwave Circuit Design Using Linear and Nonlinear Techniques*, 2<sup>nd</sup> ed., Wiley, New Jersey, 2005.
- [3] D. M. Pozar, *Microwave Engineering*, 3<sup>rd</sup> ed., Wiley, New York, 2005.
- [4] P. P. Roberts and G. E. Town, "Design of microwave filters by inverse scattering," *IEEE Trans. Micro. Theory and Tech.*, vol. 43, no. 4, pp. 739-743, Apr. 1995.
- [5] M. L. Roy, A. Perennec, S. Toutain, and C. Calvez, "The continuously varying transmission-line technique – application to filter design," *IEEE Trans. Micro. Theory and Tech.*, vol. 47, no. 9, pp. 1680-1687, Sep. 1999.
- [6] S. Y. Shi, W. J. Feng, W. Q. Che, and Q. Xue, "Novel miniaturization method for wideband filter design with enhanced upper stopband," *IEEE Microwave Theory and Techniques*, vol. 61, no. 2, pp. 817-826, Feb. 2013.
- [7] L.-H. Hsieh and K. Chang, "Compact elliptic-function low-pass filters using microstrip stepped-impedance hairpin resonators," *IEEE Trans. Microw. Theory Tech.*, vol. 51, no. 1, pp. 193-199, Jan. 2003.
- [8] A. S. Mohra, "Compact lowpass filter with sharp transition using defected ground structure," *Prog. Electromagnetic Res. Lett.*, vol. 8, pp. 83-92, 2009.
- [9] J.-I. Park, C.-S. Kim, J. Kim, and J.-S. Park, "Photonic bandgap structure for low-pass filter of wide stopband," vol. 10, no. 1, pp. 13-15, Jan. 2000.
- [10] H. Liu, Z. Li, X. Sun, and J. Mao, "A novel photonic band-gap microstrip structures for low-pass filters of wide stop-band," vol. 37, no. 6, pp. 470-472, Jun. 2003.
- [11] A. Ali. and Z. Hu, "Negative permittivity meta-material microstrip binomial low-pass filter with sharper cut-off and reduced size," *Microwaves, Antennas & Propagation, IET*, vol. 2, no. 1, pp. 15-18, Feb. 2008.
- [12] C. Miao, J. Xu, and W. Wu, "Compact wide stopband quasi-elliptic function lowpass filter using quasi-lumped elements," *Progress In Electromagnetics Research Letters*, vol. 39, pp. 151-159, 2013.
- [13] L. Li, Z.-F. Li, and J.-F. Mao, "Compact lowpass filters with sharp and expanded stopband using stepped impedance hairpin units," *IEEE Microw. Wireless Compon. Lett.*, vol. 20, no. 6, pp. 310-312, Jun. 2010.
- [14] I. Rumsey, M. Piket-May, and P. K. Kelly, "Photonic bandgap structure used as filters in microstrip circuits," *IEEE Microw. Guided Wave Lett.*, vol. 8, no. 10, pp. 336-338, Oct. 1998.
- [15] D. Ahn, J. S. Park, C. S. Kim, J. Kim, Y. Qian, and T. Itoh, "A design of the low-pass filter using the novel microstrip defected ground structure," *IEEE Trans. Microw. Theory Tech.*, vol. 49, no. 1, pp. 86-93, Jan. 2001.
- [16] M. Challal, A. Boutejdar, M. Dehmas, A. Azrar, and A. Omar, "Compact microstrip low-pass filter design with ultra-wide reject band using a novel quarter-circle DGS shape," *ACES Journal*, vol. 27, no. 10, pp. 808-815, Oct. 2012.
- [17] J.-M. Zhou, L.-H. Zhou, H. Tang, Y.-J. Yang, J.-X. Chen, and Z.-H. Bao, "Novel compact microstrip lowpass filters with wide stopband using defected ground structure," *J. of Electromagn. Waves and Appl.*, vol. 25, pp. 1009-1019, 2011.

- [18] M. Hayati and H. Abbasi, "Compact microstrip stepped-impedance lowpass filter with wide stopband using SICMRC," *IEICE Electronics Express*, vol. 9, no. 22, pp. 1742-1747, Nov. 2012.
- [19] M. Durán-Sindreu, J. Bonache, and F. Martín, "Compact elliptic-function coplanar waveguide low-pass filters using backside metallic patterns," *IEEE Microwave and Wireless Components Letters*, vol. 20, no. 11, pp. 1507-1509, Nov. 2010.
- [20] M. Hayati, A. Sheikhi, and A. Lotfi, "Compact lowpass filter with wide stopband using modified semi-elliptic and semi-circular microstrip patch resonator," *Electronics Letters*, vol. 46, no. 22, pp. 601-603, Oct. 2010.
- [21] J.-Y. Wu, Y.-H. Tseng, and W.-H. Tu, "Design of compact lowpass filter with ultra-wide stopband using thin slots," *Progress In Electromagnetics Research C*, vol. 31, pp. 137-151, Jul. 2012.
- [22] M. H. Yang, J. Xu, Q. Zhao, L. Peng, and G. P. Li, "Compact, broad-stopband lowpass filters using sirs-loaded circular hairpin resonators," *Progress In Electromagnetics Research*, 102, 95-106, 2010.
- [23] H. R. Khakzad, S. H. Sedighy, and M. K. Amirhosseini, "Design of compact SITLs low pass filter by using invasive weed optimization (IWO) technique," *Applied Computational Electromagnetics Society (ACES) Journal*, vol. 28, no. 3, pp. 228-233, Mar. 2013.
- [24] S. H. Sedighy, A. R. Mallahzadeh, M. Soleimani, and J. Rashed-Mohassel, "Optimization of printed Yagi antenna using invasive weed optimization (IWO)," *IEEE Antennas and Wireless Propagation Letters*, vol. 9, pp. 1275-1278, Jan. 2010.
- [25] A. R. Mehrabian and C. Lucas, "A novel numerical optimization algorithm inspired from invasive weed colonization," *Ecological Informatics*, vol. 1, pp. 355-366, 2006.
- [26] M. R. Ghalenoei, H. Hajimirsadeghi, and C. Lucas, "Discrete invasive weed optimization algorithm: application to cooperative multiple task assignment of UAVs, Presented at Joint 48<sup>th</sup> IEEE Conference on Decision and Control and 28<sup>th</sup> Chinese Control Conference Shanghai, available, Dec. 2009.
- [27] J. Wang, L.-J. Xu, S. Zhao, Y.-X. Guo, and W. Wu, "Compact quasi-elliptic microstrip lowpass filter with wide stopband," *Electronics Letters*, vol. 46, no. 20, pp. 1384-1385, Sep. 2010.
- [28] J.-K. Lee, D.-H. Lee, and Y.-S. Kim, "A compact lowpass filter with double step impedance shunt stub and defected ground structure for wideband rejection," *Microwave Opt. Technol. Lett.*, vol. 52, pp. 132-134, Jan. 2010.